Vibration mitigation with a nonlinear energy sink having periodically extended stiffness

K. Dekemele [1], **G. Habib** [2], **M. Loccufier** [1]
[1] Ghent University, Department of Electromechanical, Systems and Metal Engineering,
Tech lane Ghent science park 125, 9052, Ghent, Belgium
e-mail: **kevin.dekemele@ugent.be**

[2] Budapest University of Technology and Economics, Department of Applied Mechanics,
MTA-BME Lendület Machine Tool Vibration Research Group,
Műegyetem rkp. 5., H-1111, Budapest, Hungary

Abstract
Nonlinear energy sinks (NESs) are passive vibration absorbers consisting having a nonlinear interface which connects to a host system. The nonlinearity enables a 'self-tuning' property where the NES has a wider effective frequency bandwidth compared to the conventional linear tuned-mass-dampers (TMD). Typically, a hardening polynomial stiffness connection is investigated, which has been shown to have a much smaller effective energy range compared to the TMD.The NES's efficiency deteriorate depending on vibration levels, while the TMD's efficiency is independent of this. At the lower end of the energy range, a minimum level of vibrations is needed in the host system for the NES to activate. Above this threshold, the NES is efficient. At the higher end of the energy range, the efficiency of the NES slowly decreases as the vibration levels increase. Here, a radically different interface is investigated, a periodically extended stiffness characteristic. This stiffness is periodically hardening and softening. It is shown in this paper that this stiffness results in an NES with a wider energy bandwidth than the conventional NES for harmonically excitations.

1 Introduction

A nonlinear energy sink (NES) is a passive dynamic vibration absorber that is connected through a nonlinear interface to a vibrating mechanical system (the host system) [1, 2, 3, 4, 5, 6]. This nonlinear interface is usually a hardening stiffness, represented by a cubic polynomial. This nonlinear stiffness enables the NES to tackle a wider frequency range than the typical linear tuned-mass-damper (TMD) [7, 8, 9]. Furthermore, the NES has the ability to dissipate multiple frequencies under transient loading, from high to low frequency. This ability is called resonance capture cascade (RCC) [10, 7, 11, 12, 13, 14]. Under harmonically loaded host system, the NES also acts as a broadband vibration absorber. Contrary to the linear TMD, there is no creation of a second resonance when adding the NES as vibration absorber. Furthermore, it also has the ability to capture more than one resonance frequency [7] under harmonic loading. Although the NES has a larger frequency bandwidth, its performance suffers over a wide energy range. This means that as the vibration energy in the host system varies because of changing loads magnitudes, the performance deteriorates. Conversely, the TMD's efficiency is independent of this. For low energy, a minimum amount of vibration energy is required to activate the NES, the vibration threshold [6, 12, 15]. At the higher end of the energy range, the efficiency of the NES slowly decreases as the vibration levels increase.

Researchers have been able to slightly increase the efficient energy range by investigated nonlinear interfaces that are small variations on the typical hardening polynomial. For instance, by adding a negative linear component to the harderning stiffness, a bistable NES is obtained [9, 16, 17]. This paper will investigate the radically different periodically extended stiffness, which is a cubic stiffness periodically extended. It was shown in a previous work [18] that under transient loading the energy range was increased enormously

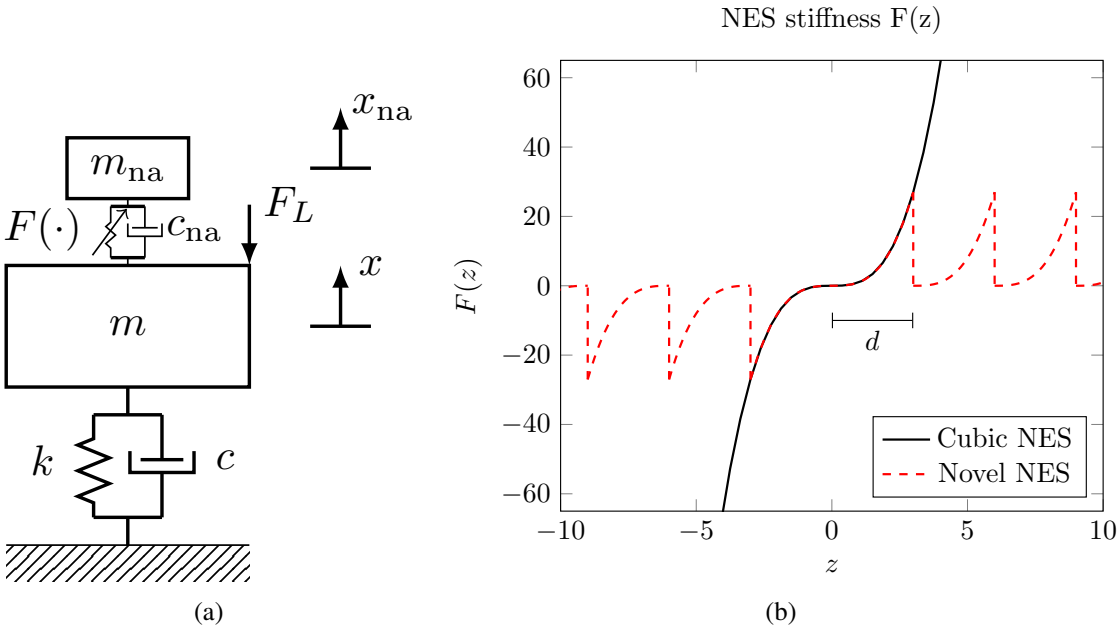

(a) (b)

Figure 1: The primary system with an NES (a) and the connecting stiffness characteristic of conventional NESs and of the proposed periodically extended NES (b).

compared to the conventional NES. In the current work, the performance of such an NES under harmonic loading of a linear host system is investigated.

The paper is structured as follows. In the next section, the system dynamics and periodically extended stiffness are presented in detail. Then, in section 3 the harmonic balancing technique is applied to obtain a nonlinear frequency response for both the host system and NES vibrations, that depends on the loading intensity. The stability of each branch in the nonlinear frequency response is also investigated. The results of section 3 are compared to a Runge-Kutta simulation in section 4 for a chosen host system. Finally, conclusions and future work are stated.

2 Model Description

The scheme of the single-degree-of-freedom host system with connected NES is presented in Figure 1a where m, c, and k are the host system's mass, damping and stiffness and where m_{na}, c_{na} and $F(\cdot)$ are the NES's mass, viscous damping and nonlinear spring characteristic. The coordinates x and x_{na} are the displacement of the host system and of the NES, respectively. Finally, a harmonic load F_L with frequency ω is exerted on the host system. The dynamical equation of the host system and NES is:

$$\begin{aligned} m\ddot{x} + c\dot{x} + kx + c_{\mathrm{na}}(\dot{x} - \dot{x}_{\mathrm{na}}) + k_{\mathrm{na}}F(x - x_{\mathrm{na}}) &= F_L\cos(\omega t) \\ m_{\mathrm{na}}\ddot{x}_{\mathrm{na}} + c_{\mathrm{na}}(\dot{x}_{\mathrm{na}} - \dot{x}) + k_{\mathrm{na}}F(x_{\mathrm{na}} - x) &= 0 \end{aligned} \tag{1}$$

where k_{na} is the proportionality factor of connecting nonlinear stiffness.
The nonlinear connecting stiffness $F(z)$, where $z = x_{\mathrm{na}} - x$, is a periodic extension in $\mathbb{R}^+$ of z^3 defined in $0 < z < d$, and an extension in $\mathbb{R}^-$ of z^3 defined in $-d < z < 0$ in order to obtain a odd characteristic:

$$F(z) = \begin{cases} (z + i \cdot d)^3 & -(i+1)d \leq z < -id \text{ with } i \in \mathbb{N}^+ \\ z^3 & -d \leq z \leq d \\ (z - i \cdot d)^3 & id < z \leq (i+1)d \text{ with } i \in \mathbb{N}^+ \end{cases} \tag{2}$$

as such d is the periodicity of the extension. This stiffness is plotted in Figure 1b for $d = 3$.

3 Harmonic balancing

The equations in (1) are divided by the primary mass m:

$$\begin{aligned} &\ddot{x} + \epsilon\omega_0\xi\dot{x} + \omega_0^2 x + \epsilon\ddot{x}_{\text{na}} = \epsilon\omega_0^2 P\cos(\omega t) \\ &\epsilon\ddot{x}_{\text{na}} + \epsilon\omega_0\xi_{\text{na}}(\dot{x}_{\text{na}} - \dot{x}) + \epsilon\omega_0^2\gamma F(x_{\text{na}} - x) + \epsilon\omega_0^2\kappa(x_{\text{na}} - x) = 0 \end{aligned} \tag{3}$$

with

$$\omega_0^2 = \frac{k}{m} \quad \epsilon = \frac{m_{\text{na}}}{m} \quad \xi_{\text{na}} = \frac{c_{\text{na}}}{m_{\text{na}}\omega_0} \quad \xi = \frac{c}{\epsilon m\omega_0} \quad \gamma = \frac{k_{\text{na}}}{m_{\text{na}}\omega_0^2} \quad P = \frac{F_L}{m_{\text{na}}\omega_0^2} \tag{4}$$

To solve the nonlinear differential equation, the harmonic balance method is adopted, which assumes that the host system and absorber vibrate only according to the forcing frequency ω. The proposed solutions are:

$$\begin{aligned} x &= A(t)e^{i\omega t} + A^*(t)e^{-i\omega t}, \quad \dot{x} = i\omega A(t)e^{i\omega t} - i\omega A^*(t)e^{-i\omega t} \\ x_{\text{na}} &= B(t)e^{i\omega t} + B^*(t)e^{-i\omega t}, \quad \dot{x}_{\text{na}} = i\omega B(t)e^{i\omega t} - i\omega B^*(t)e^{-i\omega t} \end{aligned} \tag{5}$$

where $A(t)$, $B(t) \in \mathbb{C}$, $*$ stands for complex conjugate. Deriving $2A(t)e^{i\omega t} = x - i\frac{\dot{x}}{\omega}$ and $2B(t)e^{j\omega t} = x_{\text{na}} - i\frac{\dot{x}_{\text{na}}}{\omega}$ yields after some steps:

$$\begin{aligned} \ddot{x} + \omega^2 x &= i2\omega\dot{A}e^{i\omega t} \\ \ddot{x}_{\text{na}} + \omega^2 x_{\text{na}} &= i2\omega\dot{B}e^{i\omega t} \end{aligned} \tag{6}$$

The nonlinear spring $F(z)$ is harmonically balanced (HB) with the first harmonic of its Fourier's series, $F(z) \approx f_1 e^{j\omega t}$, a procedure explained in [19]:

$$f_1(B, B^*) = \frac{\omega}{2\pi}\int_0^{\frac{2\pi}{\omega}} F\left(B(t)e^{i\omega t} + B^*(t)e^{-i\omega t}\right)e^{-i\omega t}dt \tag{7}$$

For odd functions of $F(\cdot)$ the integral (7) reduces to:

$$f_1(B, B^*) = BG(|B|) \tag{8}$$

where $G(|B|)$ is a real function [19]. The solution of integral (7) where $F(z)$ is (2) can be found in [18]. Inserting the solutions (5), (6) and (7) into (4), and keeping only the harmonics with ω gives:

$$\begin{aligned} &2\dot{A}i\omega + (\omega_0^2 - \omega^2)A + \epsilon\xi i\omega_0\omega A + \epsilon\left(2\dot{A}i\omega - \omega^2 A + 2\dot{B}i\omega - \omega^2 B\right) = \epsilon\omega_0^2\frac{P}{2} \\ &2\dot{B}i\omega + \xi_{\text{na}}i\omega_0\omega B - \omega^2 B + 2\dot{A}i\omega + \gamma\omega_0^2 BG(|B|) = \omega^2 A \end{aligned} \tag{9}$$

3.1 Nonlinear Frequency Response

It is now assumed that under harmonic forcing, the amplitudes A and B will eventually reach a steady state. As such, $\dot{A} = \dot{B} = 0$. Then, dividing by ω_0^2 and ϵ and by introducing $1 - \frac{\omega^2}{\omega_0^2} = \epsilon\sigma$, where σ expresses the proximity of the forcing frequency to the resonance frequency, yields:

$$\begin{aligned} &\sigma A + i\xi\sqrt{X}A - XA - XB = \frac{P}{2} \\ &i\xi_{\text{na}}\sqrt{X}B - XB + \gamma BG(|B|) = XA \end{aligned} \tag{10}$$

where $X = \frac{\omega^2}{\omega_0^2}$. Squaring the real and imaginary parts of the second equation of (10) yields:

$$X^2A^2 = \left(\xi_{\text{na}}^2 X + \left(-X + \gamma G(|B|)\right)^2\right)B^2 \tag{11}$$

In the second equation of (10) A is eliminated, then split according to real and imaginary parts and finally the sum of the squared real and imaginary parts gives:

$$\left(\left((X-\sigma)\left(\gamma G(|B|)-X\right)+X\xi_{\text{na}}\xi+X^2\right)^2+X\left(\xi\left(X-\gamma G(|B|)\right)+\xi_{\text{na}}\left(X-\sigma\right)\right)^2\right)B^2=\left(X\frac{P}{2}\right)^2 \tag{12}$$

Finally, the complex variables are expressed in their polar form, $A=\frac{a}{2}e^{i\alpha}$ and $B=\frac{b}{2}e^{i\beta}$ in the last two equations:

$$\begin{aligned}X^2a^2&=\left(\xi_{\text{na}}^2X+\left(-X+\gamma G(b)\right)^2\right)b^2\\ X^2P&=\left(\left((X-\sigma)\left(\gamma G(b)-X\right)+X\xi_{\text{na}}\xi+X^2\right)^2+X\left(\xi\left(X-\gamma G(b)\right)+\xi_{\text{na}}\left(X-\sigma\right)\right)^2\right)b^2\end{aligned} \tag{13}$$

Dividing the first by the second equation in (13) expressed the nonlinear frequency response of a under forcing P:

$$\frac{a^2}{P^2}=\frac{\xi_{\text{na}}^2X+\left(-X+\gamma G(b)\right)^2}{\left((X-\sigma)\left(\gamma G(b)-X\right)+X\xi_{\text{na}}\xi+X^2\right)^2+X\left(\xi\left(X-\gamma G(b)\right)+\xi_{\text{na}}\left(X-\sigma\right)\right)^2} \tag{14}$$

3.2 Stability

When computing the frequency response, it was assumed A and B reached a steady state. The stability is now investigated using multiple scales, similar to the analysis shown in [18]:

$$\begin{aligned}&A(t)=A(\tau_1,\tau_2)\quad B(t)=B(\tau_1,\tau_2)\quad \tau_0=\omega_0 t,\ \tau_1=\epsilon\omega_0 t\\ &\frac{d}{dt}=\omega_0\frac{\partial}{\partial\tau_0}+\epsilon\omega_0\frac{\partial}{\partial\tau_1}\end{aligned} \tag{15}$$

This procedure is applied to (9) and collected according to orders of ϵ:

$$\begin{aligned}&\frac{\partial A}{\partial\tau_0}=0\\ &2\omega_0\frac{\partial A}{\partial\tau_1}\omega i+\omega_0^2\sigma A+\xi i\omega_0\omega A-\omega^2A+2\omega_0\frac{\partial B}{\partial\tau_0}\omega i-\omega^2B=\omega_0\frac{P}{2}\\ &2\omega_0\frac{\partial B}{\partial\tau_0}\omega i+\xi_{\text{na}}i\omega_0\omega B-\omega^2B+\gamma\omega_0^2BG(|B|)=\omega^2A\end{aligned} \tag{16}$$

The third equation is divided by ω_0^2 and multiplied by i:

$$2\frac{\partial B}{\partial\tau_0}\sqrt{X}=-\xi_{\text{na}}\sqrt{X}B+iXB+iXA-\gamma iBG(|B|) \tag{17}$$

The linear stability near the equilibrium state $B=\bar{B}+\Delta_B$ is studied, where $\bar{B}$ are the steady state values found from computing the frequency response. The following linear system is obtained:

$$\begin{bmatrix}\dot{\Delta}_B\\ \dot{\Delta}_B^*\end{bmatrix}=\underbrace{\begin{bmatrix}a_{11}&a_{12}\\ a_{21}&a_{22}\end{bmatrix}}_{\mathbf{\Sigma}}\begin{bmatrix}\Delta_B\\ \Delta_B^*\end{bmatrix} \tag{18}$$

Table 1: Numerical values of host system and NES in numerical example

Coefficient	Value
m [kg]	1
c [Ns/m]	0.01
k [N/m]	1
m_{na} [kg]	0.02
c_{na} [Ns/m]	0.005
k_{na} [N/m^3]	0.006
d [m]	3

where

$$\begin{aligned} a_{11} &= a_{22}^* = iX - \xi_{\text{na}}\sqrt{X} - i\gamma \left.\frac{\partial(B \cdot G(B, B^*))}{\partial B}\right|_{B=\bar{B}} \\ a_{12} &= a_{21}^* = -i\gamma \left.\frac{\partial(B \cdot G(B, B^*))}{\partial B^*}\right|_{B=\bar{B}} \end{aligned} \tag{19}$$

The expressions for $\frac{\partial(B \cdot G(B,B^*))}{\partial B}$ and $\frac{\partial(B \cdot G(B,B^*))}{\partial B^*}$ were given in [18]. If an eigenvalue of $\mathbf{\Sigma}$ has a positive real part, then the fixed point $B = \bar{B}$ is unstable.

4 Numerical example

Numerical values for the system in (1) are found in Table 1. Note that the periodicity of the nonlinear stiffness is 3. Thus for $x - x_{\text{na}} < 3$, the NES will behave as the conventional NES.

This system will be subjected to a harmonic force with increasing amplitude, $P = [1, 2, 3, 4, 8, 12]$. The nonlinear frequency responses of the host system are plotted in Figure 2 and the corresponding NES vibration amplitude in Figure 3 for a range of $\omega/\omega_0 = [0.8, 1.2]$. The host system without NES is shown in nonlinear frequency responses in gray, the stable parts of (14) in black and the unstable parts in red. To verify the nonlinear frequency response obtained from harmonic balancing, the system (1) is simulated with the ODE45 simulator of MATLAB, which uses a Runge-Kutta (RK) scheme. The frequency range is divided in 200 points. The RMS value of the time series is taken and plotted on Figures 2 and 3 in light blue dotted markers, per frequency of the applied harmonic force.

4.1 Frequency responses for $P = [1, 2]$

For $P = 1$, the host system response is found on Figure 2a and the NES response on Figure 3a. The HB frequency response with NES is about 60 % lower near resonance than the host system with NES. Peculiar is the unstable branch near resonance. The result from the RK simulation follow the HB curve quit well, except for when the HB curve is unstable. The reason for this is because the RK time simulations shows that the NES performs a quasi-periodic vibration, see Figure 4a, typical for NESs near resonance conditions of the host system [20].

By doubling the load, the resulting responses in Figures 2b and 3b, the NES is able to reduce vibrations near resonance by 80 %. Again the RK simulations follows the frequency response nicely expect for the unstable branches near $\omega/\omega_0 = 1$. This is again because of the quasi-periodic vibrations of the NES, Figure 4b. A difference compared to the previous curve is that the response of the host system and the NES both show a detached resonance curve, which the RK simulation did not reach. This detached resonance curve is undesirable, as it increases the host system's vibration amplitude. Under certain initial conditions, this curve could be reached. For now, the amplitudes of the NES, as seen on Figures 3a and 3b is below the periodicity of stiffness, 3, and as such the NES still behaves as a conventional NES.

4.2 Frequency responses for $P = 3$

A difference between the conventional NES and the periodically extended stiffness NES is first seen by increasing the load P to 3 shown in Figures 2c and 3c . The frequency responses resulting from the conventional NES is shown in yellow. The host system response is quite complex. For the conventional NES, the detached resonance curve has now attached itself in Figure 2c between $\omega/\omega_0 = [0.96, 1]$ which creates a peak at 80, only a 20 % vibration reduction. This shows the well known limited energy range of the conventional NES. However, the response with novel NES is different, as the curve between $\omega/\omega_0 = [0.96, 1]$ does not reach 80, but collapses into itself. The results from the RK simulations show that host system with NES still has 60 % vibration reduction, thus proving that the novel NES has a larger amplitude range than the conventional NES. The novel NES does create a detached resonance curve in Figure 2c on the right side of the resonance, between $\omega/\omega_0 = [1, 1.02]$. The periodicity of the NES can be seen in the frequency response of the NES, Figure 3c. Here, only where the NES amplitude is above the periodicity $d = 3$, do the curves of the conventional NES and novel NES diverge. The detached resonance curve is also seen here for the novel NES.

The NES vibrations from the RK simulations do not lay perfectly on the HB curves, between $\omega/\omega_0 = [0.96, 0.99]$ and $[1.01, 1.04]$, both for the host system and NES vibrations. A RK simulation for $\omega/\omega_0 = 0.98$ in Figure 5a shows that the response goes above the periodicity of $d = 3$, shown in yellow dashed. Then, the NES vibrates with several frequencies, while HB only assumed the forcing frequency. This is why for $\omega/\omega_0 = [0.96, 0.99]$, the HB curve and RK simulation results diverge. A time simulation for $\omega/\omega_0 = 1.02$ has the typical quasi-periodic vibrations as associated with the conventional NES, as the novel NES vibrations are below $d = 3$.

4.3 Frequency responses for $P = 4$

The HB curve on the frequency response of the host system on Figure 2d has now an overal lower level than for $P = 3$, Figure 2c, which the RK simulations confirm. The maximum amplitude is 75% lower than the undamped host system. The conventional NES is only able to reduce to 15%. The detached resonance curve on the right side of resonance for $P = 3$ has now attached itself. The response for the NES is found in Figure 3d. As before, there is divergence between conventional NES and novel NES once the amplitude is above the periodicity $d = 3$. As for the host system response, the detached resonance curve has now attached itself. The RK time simulation does not follow the curve of the NES amplitude well, but this is similar to $P = 3$, where to the left the NES vibrates with several frequencies, and to the right the vibration is quasi-periodic. The time series obtained from the RK simulation for $\omega/\omega_0 = 0.99$ is presented in Figure 6a. The vibrations of the NES reach above the periodicity, resulting in several frequencies and chaotic response.

4.4 Frequency responses for $P = [8, 12]$

The load is increased even more. For $P = 8$, the host system's amplitude is given in Figure 2e and the NES amplitude in Figure 3e. The novel NES is still able to reduce half of the vibration amplitude, while the conventional NES fails mitigating the vibrations. The NES frequency response resembles a tree shape, Figure 3e. This tree shape was also found in [21] when isolated resonance curves merge. The novel NES can vibrate with a much higher amplitude than the conventional NES, as such it is able to better damp the vibrations. The RK simulations and HB match quite well for both the host system and NES. A time simulation for $\omega/\omega_0 = 1$ in Figure 6b shows a near harmonic response of the NES, while the NES stiffness has 3 hardening-softening cycles. For $P = 12$, Figures 2f, 3f and 6c the results are almost the same as for $P = 8$, but with a slight decrease of performance, only reducing 40% peak vibrations, and in increase is absorber vibration amplitude.

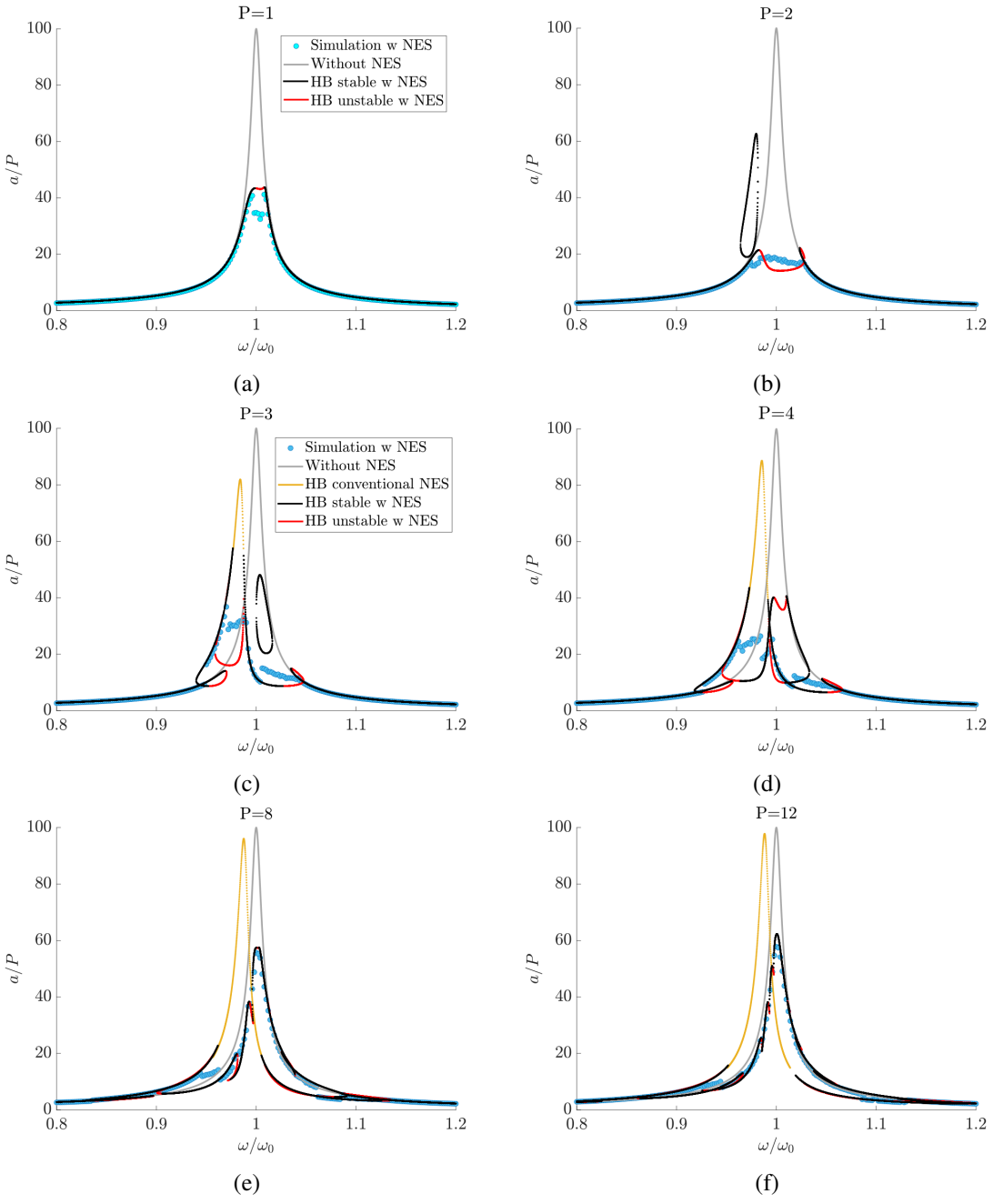

Figure 2: Nonlinear frequency responses of the host system with NES, obtained from Harmonic balancing. The excitation varies from $P = 1$ until $P = 12$.

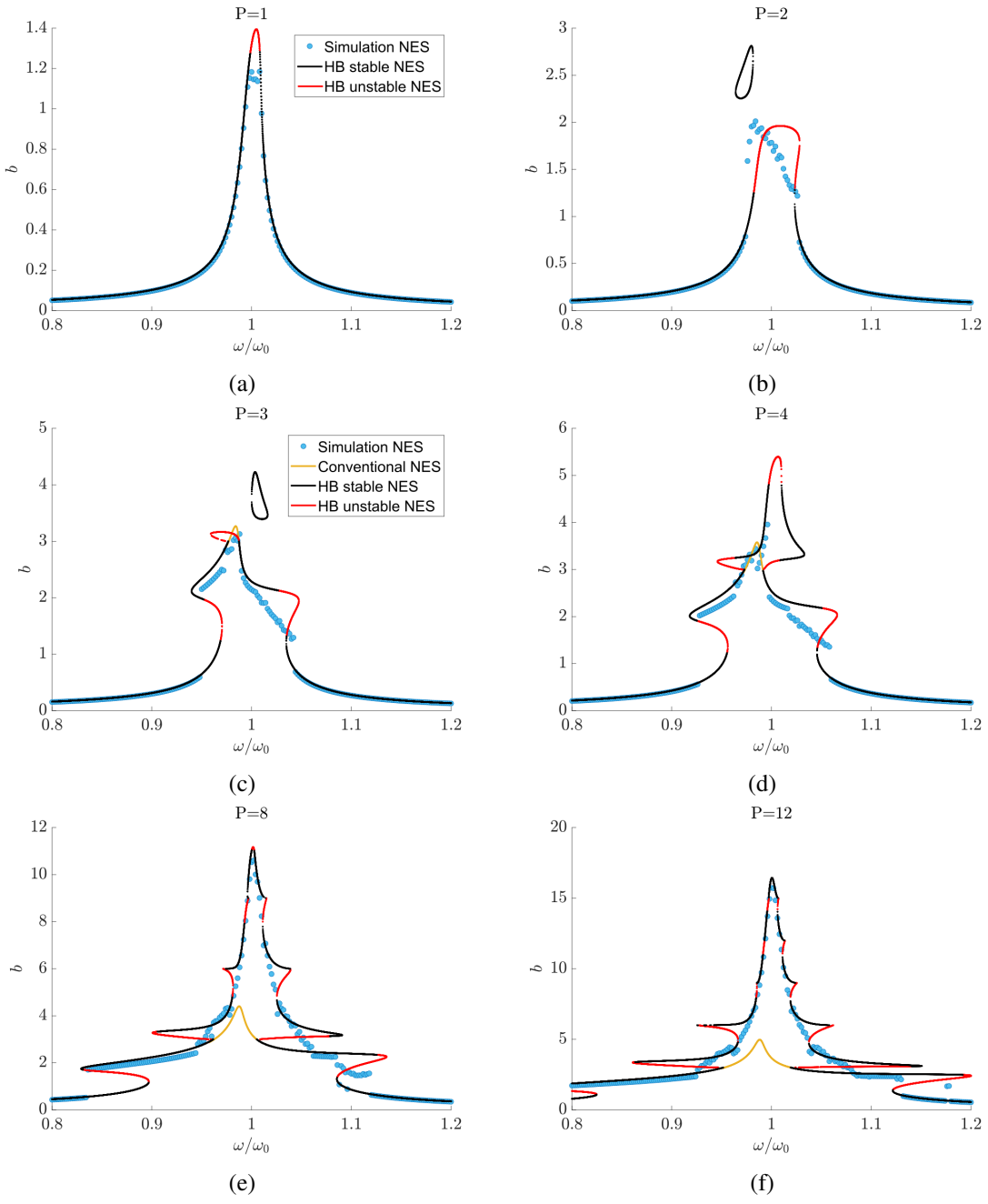

Figure 3: Nonlinear frequency responses relative NES vibration, obtained from Harmonic balancing. The excitation varies from $P = 1$ until $P = 12$.

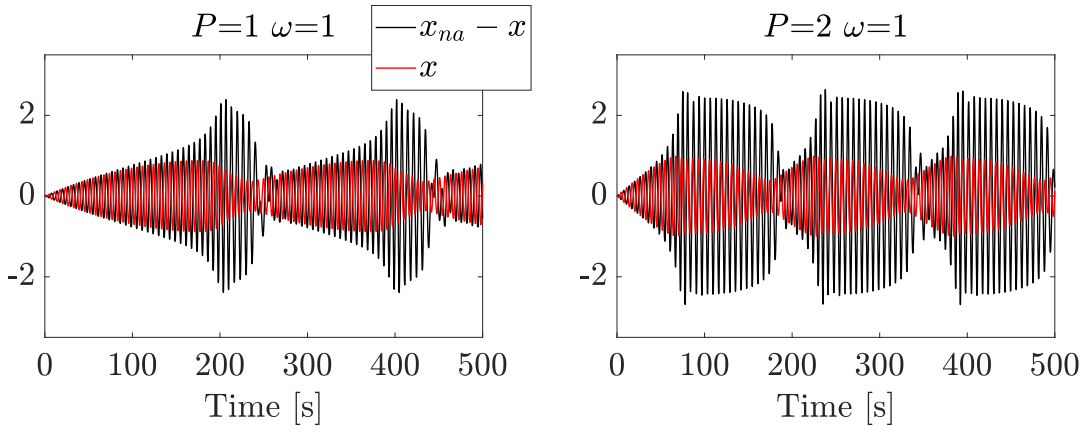

(a) (b)

Figure 4: Time series obtained from Runge-Kutta simulation for varying loads and frequency where $\omega_0 = 1$, (a) $P = 1$ and $\omega = 1$ and (b) $P = 2$ and $\omega = 1$.

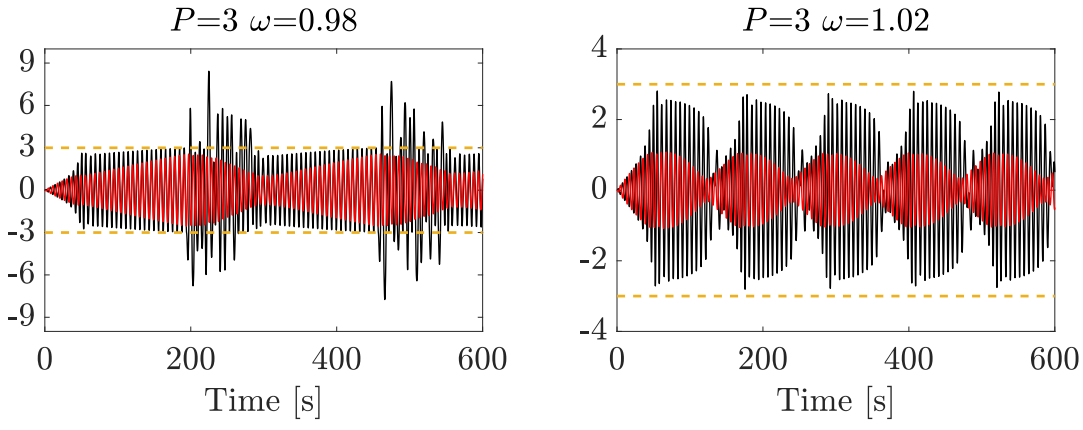

(a) (b)

Figure 5: Non-harmonic time series obtained from Runge-Kutta simulation $\omega_0 = 1$, (a) $P = 3$ and $\omega = 0.98$ and (b) $P = 3$ and $\omega = 1.02$.

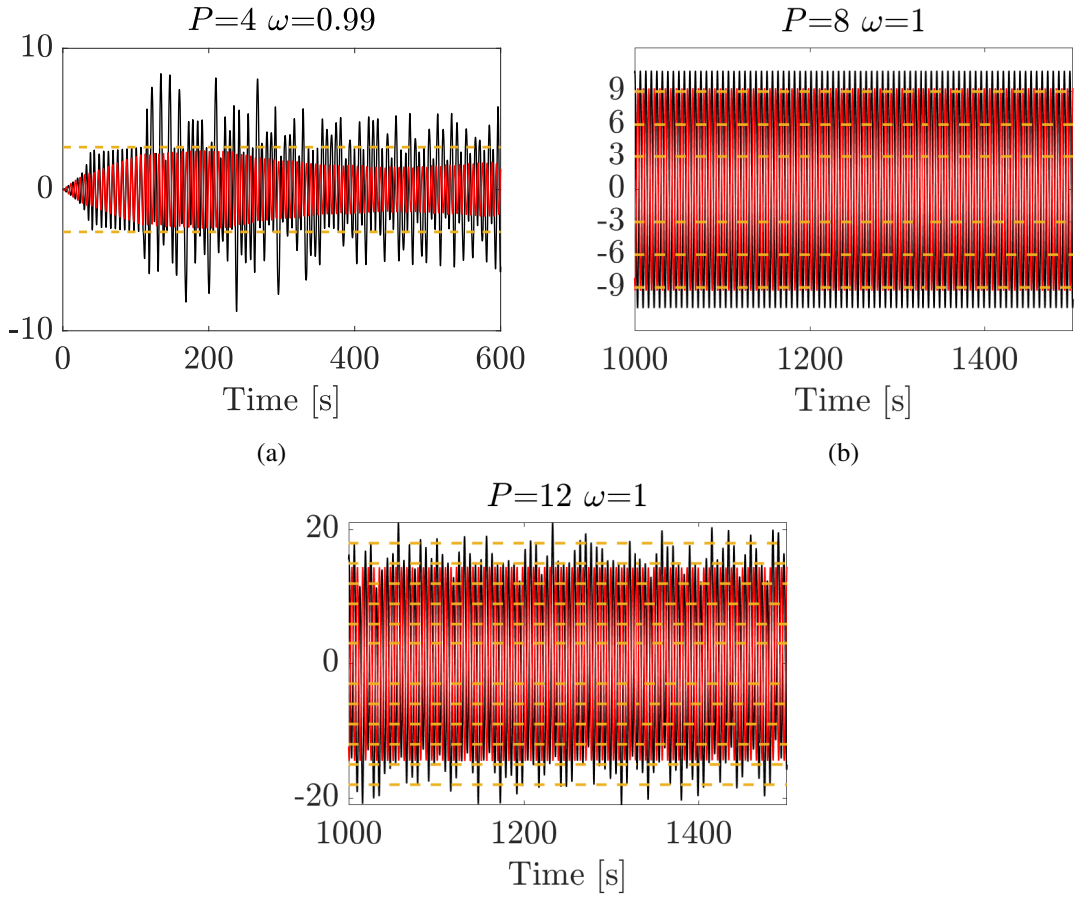

Figure 6: Time series obtained from Runge-Kutta simulation for varying loads and frequency $\omega_0 = 1$, (a) $P = 4$ and $\omega = 0.99$, (b) $P = 8$ and $\omega = 1$ and $P = 12$ and $\omega = 1$.

5 Conclusion

In this paper the performance of an NES with periodically extended stiffness in reducing harmonically induced vibrations was investigated. By applying harmonic balancing (HB), an analytical expression for the frequency response and its stability was obtained. The HB method was compared to the time series obtained from a Runge-Kutta scheme. The results matched quite well except for when the NES vibrated quasi-periodically or with multiple frequencies, which is not accounted for in the HB method. The frequency responses of the host system with novel NES was compared to the frequency response with a conventional NES. It was found that for varying loads, the novel NES is much more robust than the conventional NES. In future works the performance of the novel NES will be compared to the conventional linear vibration absorbers. Besides more complex host systems encompassing resonance frequencies will be considered.

Acknowledgements

Giuseppe Habib acknowledges the financial support of the Hungarian National Science Foundation under Grant Numbers OTKA 134496.

References

[1] O. Gendelman, L. Manevitch, A. F. Vakakis, and R. Mcloskey, "Energy pumping in nonlinear mechanical oscillators: Part i dynamics of the underlying hamiltonian systems," *J. Appl. Mech.*, vol. 68, no. 1, pp. 34–41, 2001.

[2] A. F. Vakakis, "Inducing passive nonlinear energy sinks in vibrating systems," *J. Vib. Acoust.*, vol. 123, no. 3, pp. 324–332, 2001.

[3] G. Kerschen, A. F. Vakakis, Y. S. Lee, D. M. McFarland, J. J. Kowtko, and L. A. Bergman, "Energy transfers in a system of two coupled oscillators with essential nonlinearity: 1: 1 resonance manifold and transient bridging orbits," *Nonlinear Dynamics*, vol. 42, no. 3, pp. 283–303, 2005.

[4] G. Kerschen, Y. S. Lee, A. F. Vakakis, D. M. McFarland, and L. A. Bergman, "Irreversible passive energy transfer in coupled oscillators with essential nonlinearity," *SIAM Journal on Applied Mathematics*, vol. 66, no. 2, pp. 648–679, 2005.

[5] Y. S. Lee, G. Kerschen, A. F. Vakakis, P. Panagopoulos, L. Bergman, and D. M. McFarland, "Complicated dynamics of a linear oscillator with a light, essentially nonlinear attachment," *Physica D: Nonlinear Phenomena*, vol. 204, no. 1-2, pp. 41–69, 2005.

[6] F. Petit, M. Loccufier, and D. Aeyels, "The energy thresholds of nonlinear vibration absorbers," *Nonlinear dynamics*, vol. 74, no. 3, pp. 755–767, 2013.

[7] A. F. Vakakis, O. V. Gendelman, L. A. Bergman, D. M. McFarland, G. Kerschen, and Y. S. Lee, *Nonlinear targeted energy transfer in mechanical and structural systems*. Springer Science & Business Media, 2008, vol. 156.

[8] F. Petit, M. Loccufier, and D. Aeyels, "Feasibility of nonlinear absorbers for transient vibration reduction," in *International conference on Noise and Vibration Engineering (ISMA 2010); Conference on Uncertainty in Structural Dynamics (USD 2010)*. KU Leuven. Departement Werktuigkunde, 2010, pp. 1219–1233.

[9] G. Habib and F. Romeo, "The tuned bistable nonlinear energy sink," *Nonlinear Dynamics*, vol. 89, no. 1, pp. 179–196, 2017.

[10] A. F. Vakakis, L. Manevitch, O. Gendelman, and L. Bergman, "Dynamics of linear discrete systems connected to local, essentially non-linear attachments," *Journal of Sound and Vibration*, vol. 264, no. 3, pp. 559–577, 2003.

[11] G. Kerschen, J. J. Kowtko, D. M. McFarland, L. A. Bergman, and A. F. Vakakis, "Theoretical and experimental study of multimodal targeted energy transfer in a system of coupled oscillators," *Nonlinear Dynamics*, vol. 47, no. 1, pp. 285–309, 2007.

[12] K. Dekemele, R. De Keyser, and M. Loccufier, "Performance measures for targeted energy transfer and resonance capture cascading in nonlinear energy sinks," *Nonlinear Dynamics*, vol. 93, no. 2, pp. 259–284, 2018.

[13] K. Dekemele, P. Van Torre, and M. Loccufier, "Design, construction and experimental performance of a nonlinear energy sink in mitigating multi-modal vibrations," *Journal of Sound and Vibration*, vol. 473, p. 115243, 2020.

[14] G. Habib and F. Romeo, "Tracking modal interactions in nonlinear energy sink dynamics via high-dimensional invariant manifold," *Nonlinear Dynamics*, vol. 103, no. 4, pp. 3187–3208, 2021.

[15] B. Vaurigaud, A. Ture Savadkoohi, and C.-H. Lamarque, "Targeted energy transfer with parallel nonlinear energy sinks. part i: design theory and numerical results," *Nonlinear dynamics*, vol. 66, no. 4, pp. 763–780, 2011.

[16] G.-X. Wang and H. Ding, "Mass design of nonlinear energy sinks," *Engineering Structures*, vol. 250, p. 113438, 2022.

[17] G.-X. Wang, H. Ding, and L.-Q. Chen, "Performance evaluation and design criterion of a nonlinear energy sink," *Mechanical Systems and Signal Processing*, vol. 169, p. 108770, 2022.

[18] K. Dekemele, G. Habib, and M. Loccufier, "The periodically extended stiffness nonlinear energy sink," *Mechanical Systems and Signal Processing*, vol. 169, p. 108706, 2022.

[19] O. V. Gendelman, "Targeted energy transfer in systems with non-polynomial nonlinearity," *Journal of Sound and Vibration*, vol. 315, no. 3, pp. 732–745, 2008.

[20] O. V. Gendelman and Y. Starosvetsky, "Quasi-periodic response regimes of linear oscillator coupled to nonlinear energy sink under periodic forcing," 2007.

[21] G. Habib, G. I. Cirillo, and G. Kerschen, "Isolated resonances and nonlinear damping," *Nonlinear Dynamics*, vol. 93, no. 3, pp. 979–994, 2018.